

Neural Network and Sampling Kantorovich Operators vs Traditional Denoising Techniques

Ana Maria Acu[1(✉)], Cristian Daniel Alecsa[1], Arianna Travaglini[2], and Gianluca Vinti[1,3]

[1] Department of Mathematics and Informatics, Lucian Blaga University of Sibiu, 5-7, Str. Dr. I. Raţiu, 550012 Sibiu, Romania
anamaria.acu@ulbsibiu.ro, gianluca.vinti@unipg.it

[2] Department of Physics and Geology, University of Perugia, Via A. Pascoli, 06123 Perugia, Italy
arianna.travaglini@collaboratori.unipg.it

[3] Department of Mathematics and Computer Science, University of Perugia, 1, Via Vanvitelli, 06123 Perugia, Italy

Abstract. This paper addresses the problem of image reconstruction in the presence of different types of noise, focusing on the analysis and comparison of several filtering techniques. In particular, Neural Network (NN) operators and sampling Kantorovich (SK) operators are investigated alongside a variety of classical and advanced filtering methods, including linear, nonlinear, and state-of-the-art approaches commonly adopted in the literature. The performance of the considered methods is evaluated through widely used quantitative metrics. The experimental analysis highlights the ability of NN and SK operators to provide accurate and stable reconstructions, ensuring the effectiveness and versatility of the proposed operators across different noise conditions.

Keywords: Neural network operators · sampling Kantorovich operators · Image filtering · Image smoothing

1 Introduction

In recent years, the study of advanced approximation techniques for image processing has attracted significant attention, particularly in relation to operator-based methods and their applications to image reconstruction, rescaling, and denoising. These issues are especially critical in domains where accurate visual information is essential, such as medical imaging, remote sensing, and scientific visualization, where reliable data is crucial for analysis, interpretation, and decision-making.

Over the years, a variety of filtering techniques have been developed to reduce noise and improve the overall quality of images. Each filter is generally designed to address specific types of noise—for instance, Gaussian filters are commonly

© The Author(s), under exclusive license to Springer Nature Switzerland AG 2027
O. Gervasi et al. (Eds.): ICCSA 2026 Workshops, LNCS 16763, pp. 124–141, 2027.
https://doi.org/10.1007/978-3-032-30530-5_8

applied to mitigate Gaussian noise. However, the limited adaptability of these classical filters to different noise models represents a significant drawback, motivating the development of more flexible and general approaches.

Among the most promising approaches are neural network (NN) operators, which have been extensively investigated due to their strong connections with the theory of artificial neural networks (see [7–10,15,20]). The NN operators activated by a sigmoidal function σ and acting on $f : I \to \mathbb{R}$ are defined as

$$F_n(f, \mathbf{x}) := \frac{\sum\limits_{k \in \mathcal{A}_n} f\left(\frac{\mathbf{k}}{n}\right) \Psi_\sigma(n\mathbf{x} - \mathbf{k})}{\sum\limits_{k \in \mathcal{A}_n} \Psi_\sigma(n\mathbf{x} - \mathbf{k})},$$

for every $\mathbf{x} \in I$ and $\mathbf{k} = (k_1, k_2, \ldots, k_d)$, where $I := \prod\limits_{i=1}^{d} [a_i, b_i]$ is a d-dimensional interval belonging to $\mathbb{R}^d$, $\mathcal{A}_n := \{\mathbf{k} \in \mathbb{Z}^d : \lceil na_i \rceil \leq k_i \leq \lfloor nb_i \rfloor \text{ for } i = 1, \ldots, d\}$, and where the symbols $\lfloor \cdot \rfloor$ and $\lceil \cdot \rceil$ denote the floor and ceiling functions, respectively (see, e.g., [14]).

Alongside NN-based approaches, sampling Kantorovich (SK) operators represent another powerful tool for image reconstruction and approximation. Originally introduced in [4] in the univariate setting and later extended to the multidimensional case in [13], these operators are defined as

$$(SK_w f)(\mathbf{x}) := \sum_{\mathbf{k} \in \mathbb{Z}^d} \chi(w\mathbf{x} - \mathbf{k}) \left[w^d \int\limits_{R^w_{\mathbf{k}}} f(\mathbf{u})\, d\mathbf{u} \right], \quad \mathbf{x} \in \mathbb{R}^d,$$

where χ is the kernel of the operator and $f : \mathbb{R}^d \to \mathbb{R}$ is a locally integrable function such that the series converges for every $\mathbf{x} \in \mathbb{R}^d$. SK operators provide a powerful generalization of the classical sampling framework, extending it to functions that may be discontinuous, and have been studied in various functional settings, including Orlicz spaces. They have proven particularly effective in handling real-world imaging problems (see, e.g., [11,22,25,27,28]). Indeed, both SK and NN operators are used as smoothing filters due to their low-pass filtering behavior given by their convolutive nature (see [1]). To evaluate their effectiveness and versatility in reconstructing images corrupted by various types of noise, we perform a comparative analysis considering three different and commonly encountered types of noise—Gaussian, Poisson, and Speckle—to ensure that the comparison reflects the methods' adaptability across different noise conditions (see [19,31]). The reconstructed images obtained through SK and NN operators are then compared with those produced by classical image filtering techniques, such as Gaussian, Wiener, BM3D, Median, Bilateral, Non-Local Means (NLM), a combination of Variance Stabilizing Transform (VST) and Non-Local Means, Lee, Frost, Log-Wiener and Wiener-Anscombe filters (see, e.g., [3,6,16–18,21,23,24,26,30]).

To quantitatively assess the quality of the reconstructed images, several widely used similarity measures are employed, including the Root Mean Square

Error (RMSE), the Structural Similarity Index (SSIM), the Feature Similarity Index (FSIM), and the Feature-based Loss Index for Perceptual quality (ꟻLIP) (see [2,5,29,32]). Unlike classical pixel-wise error metrics such as RMSE, SSIM captures structural information by accounting for luminance, contrast, and local correlations. These metrics provide complementary measures of image fidelity, perceptual quality, and structural consistency, allowing for a comprehensive evaluation of the denoising performance of each method.

Overall, this work underline the effectiveness of operator-based approximation methods, such as NN and SK operators, in modern image processing. By integrating theoretical foundations from approximation theory with practical algorithmic design and evaluation through established metrics, these approaches provide robust and flexible tools for tackling complex tasks such as image denoising and reconstruction across different noise models.

2 Algorithmic Framework

This section presents the mathematical and algorithmic framework for image reconstruction and resizing based on multivariate neural network (NN) and sampling Kantorovich (SK) operators. Both approaches are formulated in a continuous setting and can be naturally applied to grayscale images interpreted as functions over multidimensional domains.

The multivariate NN operator considered, activated by a sigmoidal function σ, has been studied, e.g., in [1,14] and it is defined for $n \in \mathbb{N}^+$, as

$$F_n(f,\mathbf{x}) := \frac{\sum\limits_{k\in\mathcal{A}_n} f\left(\frac{\mathbf{k}}{n}\right)\Psi_\sigma(n\mathbf{x}-\mathbf{k})}{\sum\limits_{k\in\mathcal{A}_n}\Psi_\sigma(n\mathbf{x}-\mathbf{k})}, \quad \frac{\mathbf{k}}{n} := \left(\frac{k_1}{n},\ldots,\frac{k_d}{n}\right), \quad \text{(NN\_Operator)}$$

where $f : I \to \mathbb{R}$, with $I := \prod\limits_{i=1}^{d}[a_i,b_i]$ is a d-dimensional interval belonging to $\mathbb{R}^d$, and $\mathcal{A}_n := \{\mathbf{k}\in\mathbb{Z}^d : \lceil na_i\rceil \le k_i \le \lfloor nb_i\rfloor \text{ for } i=1,\ldots,d\}$. In addition, the sigmoidal function $\sigma : \mathbb{R}\to\mathbb{R}$ satisfies $\lim\limits_{x\to-\infty}\sigma(x)=0$ and $\lim\limits_{x\to+\infty}\sigma(x)=1$, along with the following assumptions:

(Σ_1) the function $x \to \sigma(x)-\frac{1}{2}$ is odd.
(Σ_2) $\sigma \in C^2(\mathbb{R})$ is concave for $x \ge 0$.
(Σ_3) $\sigma(x) = \mathcal{O}\left(\frac{1}{|x|^{1+\alpha}}\right)$ as $x\to-\infty$, for some $\alpha>0$.

The density function associated to σ is defined, for $x\in\mathbb{R}$, as

$$\phi_\sigma(x) := \frac{1}{2}\left[\sigma(x+1)-\sigma(x-1)\right]$$

and the multivariate kernel function Ψ_σ is constructed by means of the tensor product of the density functions, namely

$$\Psi_\sigma(\mathbf{x}) := \prod_{i=1}^{d} \phi_\sigma(x_i).$$

Within this framework, the NN operator reconstructs the function f by means of normalized weighted combinations of sampled values. Each reconstructed point is obtained as a weighted average of sampled values, where the weights are determined by the kernel Ψ_σ, thus preserving local image features while ensuring numerical stability. Note that, due to a mere typo, in [1] the rectified linear unit function (ReLU) is denoted using the symbol of a sigmoidal function, although it is not one.

An alternative reconstruction strategy is provided by SK operators introduced in [4], originally to deal with one-dimensional discontinuous signals and recently studied in a modified version to better address the problem of signals affected by noise (see [12]). The multivariate generalization of these operators was proposed in [13], which allows the application of the framework of SK operators to image processing. In this setting, the family of sampling Kantorovich operators $(SK_w)_{w>0}$ is given by

$$(SK_w f)(\mathbf{x}) := \sum_{\mathbf{k}\in\mathbb{Z}^d} \chi(w\mathbf{x}-\mathbf{k}) \left[w^d \int_{R_{\mathbf{k}}^w} f(\mathbf{u})\, d\mathbf{u} \right], \quad \mathbf{x}\in\mathbb{R}^d,\ w>0, \tag{SK_operator}$$

where $f : \mathbb{R}^d \to \mathbb{R}$ is a locally integrable, representing the signal of the image, such that the series converges for all $\mathbf{x} \in \mathbb{R}^d$. Here, the sets

$$R_{\mathbf{k}}^w := \prod_{i=1}^{d} \left[\frac{k_i}{w}, \frac{k_i+1}{w} \right]$$

denote the regions over which the local averages of f are computed. In addition, the kernel function $\chi : \mathbb{R}^d \to \mathbb{R}$ is required to satisfy the following conditions:

(χ_1) The kernel χ belongs to $L^1(\mathbb{R}^d)$ and it is bounded in a neighborhood of the origin of $\mathbb{R}^d$.

(χ_2) The kernel forms a partition of unity, i.e., $\sum_{\mathbf{k}\in\mathbb{Z}^d} \chi(\mathbf{x}-\mathbf{k}) = 1$ for all $\mathbf{x}\in\mathbb{R}^d$.

(χ_3) There exists $\beta > 0$ such that the discrete absolute moment of order $\beta > 0$ is finite, namely $m_\beta(\chi) := \sup_{\mathbf{u}\in\mathbb{R}^d} \sum_{\mathbf{k}\in\mathbb{Z}^d} |\chi(\mathbf{u}-\mathbf{k})| \cdot \|\mathbf{u}-\mathbf{k}\|_2^\beta < +\infty$.

A fundamental difference between the NN operator and the SK operator mainly relies on the fact that, in the latter mentioned, the pointwise samples are replaced by the integral mean over each region, which smooths local variations and reduces time-jitter errors. Therefore, the SK algorithm introduces inherent regularization, yielding robust reconstructions, especially in the presence of noise. Therefore, the SK operator offers a stable and regularized reconstruction framework with respect to the images corrupted with different types of input noise.

For implementation purposes, a grayscale image can be interpreted as a matrix $A = (a_{ij})_{i,j=1,\ldots,m}$, by means of which it is possible to construct the so called image function I as:

$$I(x,y) := \sum_{i=1}^{m}\sum_{j=1}^{m} a_{ij}\mathbf{1}_{ij}(x,y)$$

for every $(x,y) \in \mathbb{R}^2$, where the indicator function $\mathbf{1}_{ij}$ is defined as

$$\mathbf{1}_{ij}(x,y) = \begin{cases} 1, & \text{if } (x,y) \in (i-1,i] \times (j-1,j], \\ 0, & \text{otherwise.} \end{cases}$$

Therefore, the function I (serving as f) can be approximated using two-dimensional NN operators as well as SK operators. This can be achieved by appropriately choosing a sigmoidal function in the NN setting and a kernel function in the SK setting, as discussed earlier. The proposed methods have been implemented in MATLAB©, providing a computational framework for image reconstruction and resizing.

The implementation of the NN operator described in Algorithm 1 begins by taking a grayscale image and preparing it for upscaling or reconstruction, based on the chosen refinement factor n and scale factor R. The input image is first replicated using the Kronecker tensor product, considering the parameter n, in order to create a fine-grid intermediate representation. A sampling grid is then generated, and a kernel function is evaluated to determine the contribution of the neighboring pixel. The algorithm identifies the effective kernel support by including only the non-zero terms. Finally, the creation of image and kernel slices are created while respecting image boundaries, and their weighted contributions are combined to produce the upscaled or reconstructed output image. In contrast, the SK-based implementation, in which the reconstruction process

Algorithm 1 `NN_Operator`

Objective: Reconstructing or resizing the original image I_{in} by means of the multivariate *NN operator* based on kernels constructed using sigmoidal functions.

Inputs: Original image I_{in} of size $H_{in} \times W_{in}$, parameter $n \in \mathbb{N}^+$, scaling factor $R \geq 1$.

- ▷ Choice and definition of the kernel Ψ_σ.
- ▷ Size of the output image: $H_{out} \times W_{out}$, where $H_{out} = R \cdot H_{in}$ and $W_{out} = R \cdot W_{in}$.
- ▷ Computation of the matrices of the sample values.
- ▷ Definition of the vectors containing the arguments of Ψ_σ.
- ▷ Definition of the reconstruction grid.

Iteration: Summation over $\mathbf{k}$ of all non-zero terms of the form $\Psi_\sigma(n\mathbf{x}-\mathbf{k})I_{in}\left(\frac{k}{n}\right)$, normalized by $\Psi_\sigma(n\mathbf{x}-\mathbf{k})$, for each point x belonging to the reconstruction grid, according to the formula (NN_Operator).

Output: Reconstructed image I_{out} of size $H_{out} \times W_{out}$.

Algorithm 2 `SK_Operator`

Objective: Reconstructing or resizing the original image I_{in} by means of the multivariate *SK operator* constructed using kernel functions.

Inputs: Original image I_{in} of size $H_{in} \times W_{in}$, parameter $w \in \mathbb{N}^+$, scaling factor $R \geq 1$.

- ▷ Choice and definition of the kernel χ.
- ▷ Size of the output image: $H_{out} \times W_{out}$, where $H_{out} = R \cdot H_{in}$ and $W_{out} = R \cdot W_{in}$.
- ▷ Computation of the matrices of the sample values.
- ▷ Definition of the vectors containing the arguments of χ.
- ▷ Definition of the reconstruction grid.

Iteration: Summation over $\mathbf{k}$ of all non-zero terms of the form $\chi(w\mathbf{x} - \mathbf{k}) \left[w^d \int\limits_{R^w_{\mathbf{k}}} I_{in}(\mathbf{u})\, d\mathbf{u} \right]$, for each point $\mathbf{x}$ belonging to the reconstruction grid, according to the formula (SK_operator).

Output: Reconstructed image I_{out} of size $H_{out} \times W_{out}$.

is described in Algorithm 2, computes local averages of the image over subregions and combines them using kernel-based weights. This procedure naturally incorporates smoothing and leads to improving stability in noisy environments.

3 Experimental Data

The test images adopted in this paper are: "autumn.png" (345 × 206), "cameraman.png" (256 × 256), "lena.png" (200 × 200), "moon.png" (358 × 537), and "onion.png" (198 × 135). These images were selected to exhibit different characteristics such as size, brightness, texture, and structural complexity, allowing for a comprehensive evaluation of the denoising algorithms under varied conditions.

To study the filtering process and assess the performance of NN and SK operators, the original images were corrupted with three types of noise commonly encountered in real-world applications: Gaussian, Poisson, and Speckle noise. The noise corruption was implemented using MATLAB® with the following parameters: Gaussian noise with mean 0 and variance 0.05, Speckle noise with variance 0.04, and Poisson noise with standard parameters. Figure 1 presents both the original images and their corrupted versions for each noise type.



Fig. 1. Original test images (first column) and their corrupted versions with Gaussian (second column), Poisson (third column), and Speckle noise (fourth column).

4 NN and SK Optimization

After generating the noisy versions of the reference images, the next step was to optimize the filtering operators to achieve the best possible restoration of the original images. Since both SK and NN operators are parameter-dependent, their performance is strongly determined by the specific combination of parameters used. To enable comparisons, the scaling factor R has been set to 1 for both NN and SK algorithms.

For the NN operators, we tested all activation functions and network parameters to identify configurations that minimize the reconstruction error while preserving image structures. The density functions considered (see, e.g., [1]), indexed by the parameter k, are those ones constructed by using the following sigmoidal functions: hyperbolic tangent function ($k = 1$), logistic function ($k = 2$), ramp function ($k = 3$) and B-spline-based functions of orders 2–4 ($k = 4, 5, 6$). The parameter n controls the density of sampling points in the operator.

For the SK operators, the bandwidth parameter w determines the degree of smoothing applied to the image. The kernel used in all experiments is the

Jackson-type kernel, which proved to be well-suited for applications (see, e.g., [11,25,27]).

To identify the optimal parameters, we evaluated multiple quality indices (SSIM, RMSE, FSIM, and ꟻLIP) for each filtered image by comparing it with the original version. The images were normalized to the dynamic range $[0, 1]$, so that the results of all indices belong to the interval $[0, 1]$ too. To ensure consistency when computing an overall average, we considered $1-$RMSE and $1-$ꟻLIP so that higher values uniformly indicate better performance across all metrics. We then calculated the mean of these four normalized indices, referred to as the *index mean*. The optimal parameters for each image and noise type are those that maximize this index mean.

Table 1 summarizes the optimal parameter values obtained for each test image and noise type combination.

Table 1. Optimal parameters for SK and NN operators across different images and noise types.

Image	Noise Type	SK: w	NN: n	NN: k
Cameraman	Gaussian	4	1	2
	Poisson	16	3	2
	Speckle	9	2	2
Lena	Gaussian	5	1	2
	Poisson	17	4	2
	Speckle	10	2	2
Moon	Gaussian	4	1	2
	Poisson	11	2	2
	Speckle	6	1	2

From the optimization results, several patterns emerge. For NN operators, the logistic activation function ($k = 2$) consistently yields the best performance across all images and noise types, with the optimal value of n ranging between 1 and 4 depending on the specific noise characteristics. Lower values of n (typically $n = 1$) are optimal for Gaussian noise, while Poisson noise generally requires slightly higher values ($n = 2$ to $n = 4$). Speckle noise is optimally filtered for $n = 1$ or $n = 2$.

For SK operators, the optimal bandwidth parameter w exhibits greater variability depending on the noise type. Gaussian noise is best handled with relatively low values ($w = 4$ or $w = 5$), which provide sufficient smoothing without excessive blurring. Poisson noise, characterized by signal-dependent variance, requires higher values of w (ranging from $w = 11$ to $w = 17$) to achieve effective denoising. Speckle noise shows intermediate optimal values ($w = 6$, $w = 9$ or $w = 10$). These results are consistent with the theoretical requirements: values of w that are too high cause the reconstruction to converge toward the noisy

image, while values that are too low produce excessively blurred results with insufficient noise reduction.

5 Filtered Images

The noisy images were filtered not only using the algorithms implemented in the section above, but also using known filters, such as the Gaussian, Wiener, BM3D, Median, Bilateral, Non-Local Means (NLM), a combination of Variance Stabilizing Transform (VST) and Non-Local Means, Lee, Frost, Log-Wiener and Wiener-Anscombe filters (see, e.g., [3,6,16–18,21,23,24,26,30]), with the aim of comparing the results with NN and SK operators. The images "cameraman.png", "lena.png" and "moon.png" are more representative of the characteristics of the dataset, therefore we take them as sample for this paper. Specifically, the *Cameraman* image contains well-defined edges and structured details, making it suitable for evaluating edge detection and filtering performance. The *Lena* image offers a balanced combination of smooth regions and complex textures, which is particularly useful for assessing compression and denoising algorithms. Finally, the *Moon* image is characterized by irregular natural textures and gradual intensity variations, making it appropriate for testing performance on less structured, real-world patterns.

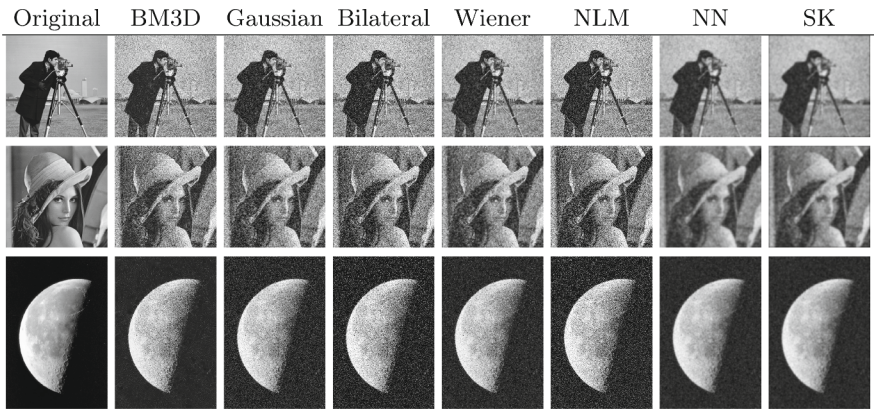

Fig. 2. The test images corrupted by Gaussian noise and then filtered using the study's selected filters for this type of noise. On the left the reference images followed by the filtered images.

The images corrupted by Gaussian noise were filtered using the NN and SK operators, in order to verify their efficiency, and other filters such as the BM3D filter, the Gaussian filter, the Bilateral filter, the Wiener filter and the Non-Local Means (NLM) filter. Figure 2 presents the filtered images corresponding to Gaussian noise, while Fig. 3 presents the filtered images corresponding to Poisson

noise, which were filtered using the NN and SK operators and other employed filters for this type of noise, such as the BM3D, the Median, the Wiener-Anscombe filter, and a combination of Variance Stabilizing Transform (VST) and NLM.

Finally, the filters used for the Speckle noise are the BM3D filter, Lee filter, Frost filter and Log-Wiener filter, along with NN and SK operators. The results are shown in Fig. 4.

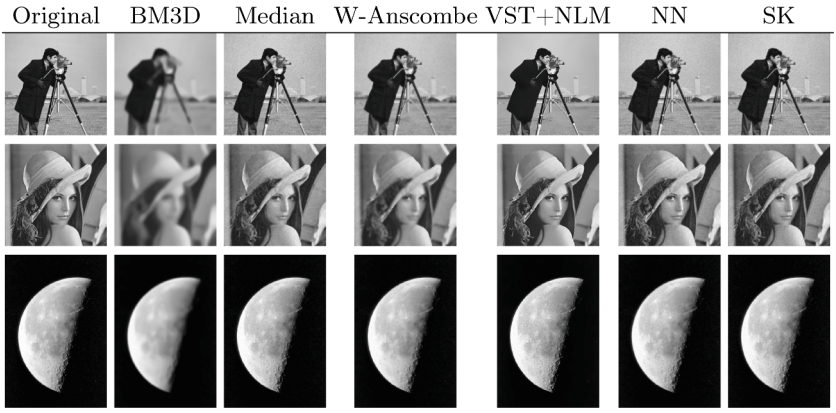

Fig. 3. The test images corrupted by Poisson noise and then filtered using the study's selected filters for this type of noise. On the left the reference images followed by the filtered images.

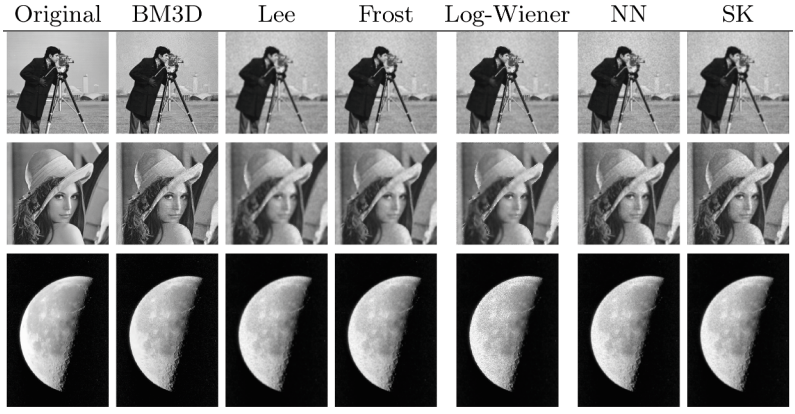

Fig. 4. The test images corrupted by Speckle noise and then filtered using the study's selected filters for this type of noise. On the left the reference images followed by the filtered images.

6 Comparison of the Results

The filtered images are compared with the original images using SSIM, RMSE, FSIM and ꟻLIP indices (see [2,5,29,32]). They were evaluated using MATLAB® formulas, except for the FSIM that was implemented using the code given in [32] and the ꟻLIP index that was calculated using the implementation in [2]. The indices reported for NN and SK algorithms correspond to the best results obtained after the optimization procedure (see Sect. 4). The following tables report the results obtained when filtering images corrupted by Gaussian, Poisson, and Speckle noise. For each noise type, a single table groups the results across all reference images. The columns report the filters used during the elaboration, while the rows are organized by image and quality index.

Table 2. Results obtained filtering images corrupted by Gaussian noise. Each row group corresponds to a reference image; the columns report the quality indices obtained comparing the reference image with each filtered version.

		BM3D	Gaussian	Bilateral	Wiener	NLM	NN	SK
Autumn	↑ **SSIM**	0.2352	0.2584	0.1793	0.3847	0.1637	0.5780	0.5407
	↓ **RMSE**	0.1408	0.1251	0.1741	0.0933	0.1882	0.0764	0.0802
	↑ **FSIM**	0.6333	0.6220	0.5709	0.7118	0.5499	0.7587	0.7527
	↓ **ꟻLIP**	0.2294	0.2259	0.2627	0.2068	0.2791	0.2019	0.2077
Cameraman	↑ **SSIM**	0.2194	0.2361	0.1777	0.3321	0.1655	0.5417	0.5405
	↓ **RMSE**	0.1642	0.1338	0.1876	0.0988	0.2016	0.0874	0.0950
	↑ **FSIM**	0.5794	0.5753	0.5301	0.6624	0.5102	0.7344	0.7141
	↓ **ꟻLIP**	0.2261	0.2311	0.2604	0.2123	0.2764	0.1993	0.2139
Lena	↑ **SSIM**	0.2351	0.2752	0.1950	0.3984	0.1790	0.5967	0.5794
	↓ **RMSE**	0.1625	0.1318	0.1860	0.0955	0.2001	0.0779	0.0791
	↑ **FSIM**	0.5845	0.5859	0.5294	0.6944	0.5068	0.7981	0.7914
	↓ **ꟻLIP**	0.2408	0.2285	0.2729	0.2039	0.2923	0.1988	0.2015
Moon	↑ **SSIM**	0.1591	0.0916	0.0604	0.1546	0.0503	0.3691	0.3910
	↓ **RMSE**	0.1153	0.1243	0.1591	0.1051	0.1743	0.0794	0.0780
	↑ **FSIM**	0.5850	0.4397	0.3942	0.5556	0.3587	0.8366	0.8505
	↓ **ꟻLIP**	0.2368	0.2919	0.3313	0.2578	0.3597	0.2330	0.2289
Onion	↑ **SSIM**	0.1423	0.1877	0.1174	0.3413	0.1047	0.6829	0.6787
	↓ **RMSE**	0.1623	0.1304	0.1860	0.0874	0.2009	0.0534	0.0622
	↑ **FSIM**	0.4857	0.5042	0.4420	0.6398	0.4183	0.8300	0.8162
	↓ **ꟻLIP**	0.2337	0.2161	0.2614	0.1903	0.2804	0.1630	0.1760

The analysis of Table 2 shows that the SSIM index is closest to 1 when using the NN or SK algorithms, regardless of the reference image considered. Similarly, the RMSE values are closer to zero for these two methods, indicating better pixel-wise similarity with respect to the original images. The FSIM index also attains its best values with NN and SK filtering, and the ꟻLIP index confirms this trend, with lower values—i.e., smaller perceptual error—consistently achieved by the same two approaches. These outcomes support the initial hypothesis, confirming the effectiveness of the proposed methods across all tested images. The ꟻLIP index produces an error map that precisely represents the perceived difference between the two images at each pixel in terms of its magnitude. Typically, lower error values are represented by darker or cooler colors (e.g., blue), indicating high similarity, while higher error values correspond to brighter or warmer colors (e.g., yellow or red), highlighting regions where significant discrepancies occur. Therefore, predominantly blue regions in the error map indicate that the filtering method effectively preserves the original image content, whereas the presence of warmer colors reveals areas of degradation or loss of detail.

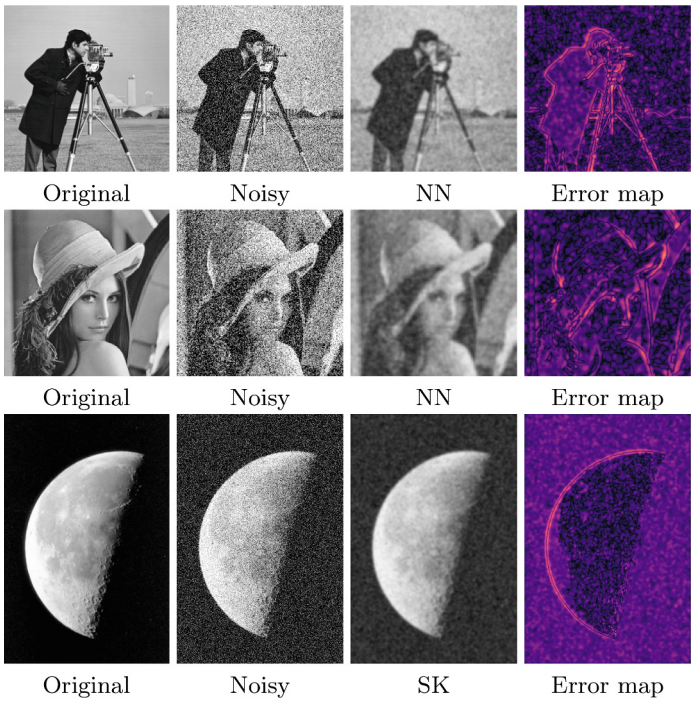

Fig. 5. On the left the reference images, in the center the image with Gaussian noise and the best filtered images, on the right the ꟻLIP error map obtained.

In Fig. 5, the ꟻLIP error maps of the best filtering results are presented for each image considered in the Gaussian noise case.

Table 3. Results obtained filtering images corrupted by Poisson noise. Each row group corresponds to a reference image; the columns report the quality indices obtained comparing the reference image with each filtered version.

		BM3D	Median	W-Anscombe	VST+NLM	NN	**SK**
Autumn	↑ **SSIM**	0.5793	0.7541	0.6965	0.9058	0.8199	0.8029
	↓ **RMSE**	0.0771	0.0437	0.0545	0.0227	0.0337	0.0321
	↑ **FSIM**	0.6585	0.8872	0.8021	0.9410	0.9036	0.9041
	↓ **ꟻLIP**	0.1590	0.0792	0.0969	0.0556	0.0711	0.0707
Cameraman	↑ **SSIM**	0.6396	0.7540	0.7659	0.8955	0.7997	0.7785
	↓ **RMSE**	0.0912	0.0478	0.0481	0.0238	0.0404	0.0374
	↑ **FSIM**	0.6836	0.8959	0.8377	0.9341	0.8951	0.8957
	↓ **ꟻLIP**	0.1492	0.0788	0.0875	0.0511	0.0743	0.0752
Lena	↑ **SSIM**	0.6088	0.8163	0.7541	0.9009	0.8464	0.8447
	↓ **RMSE**	0.0828	0.0378	0.0485	0.0233	0.0304	0.0312
	↑ **FSIM**	0.7404	0.9230	0.8601	0.9392	0.9296	0.9291
	↓ **ꟻLIP**	0.1853	0.0742	0.0982	0.0617	0.0657	0.0676
Moon	↑ **SSIM**	0.8088	0.8971	0.9066	0.8304	0.9251	0.9284
	↓ **RMSE**	0.0291	0.0159	0.0157	0.0257	0.0168	0.0145
	↑ **FSIM**	0.8171	0.9329	0.9197	0.8705	0.9399	0.9442
	↓ **ꟻLIP**	0.0645	0.0332	0.0325	0.0335	0.0336	0.0310
Onion	↑ **SSIM**	0.7357	0.8675	0.8444	0.9185	0.8979	0.8683
	↓ **RMSE**	0.0554	0.0242	0.0316	0.0192	0.0253	0.0278
	↑ **FSIM**	0.8009	0.9340	0.8953	0.9497	0.9303	0.9264
	↓ **ꟻLIP**	0.1467	0.0622	0.0764	0.0595	0.0654	0.0675

Table 3 reveals a more nuanced picture compared to the Gaussian case. The VST+NLM method achieves the best index values across most images and metrics, attaining the highest SSIM, lowest RMSE, highest FSIM, and lowest ꟻLIP scores on Autumn, Cameraman, Lena, and Onion. The NN and SK operators, while not consistently topping the rankings, frequently appear as the second-best performers and remain competitive throughout. On the Moon image, in particular, the SK filter attains the best values for all four indices, with NN ranking second. Notably, the absolute values of the ꟻLIP index across the entire table are significantly lower than those obtained in the Gaussian noise case. The corresponding error maps appear predominantly blue, indicating a high degree of similarity between the filtered and original images when correcting Poisson noise (Fig. 6).

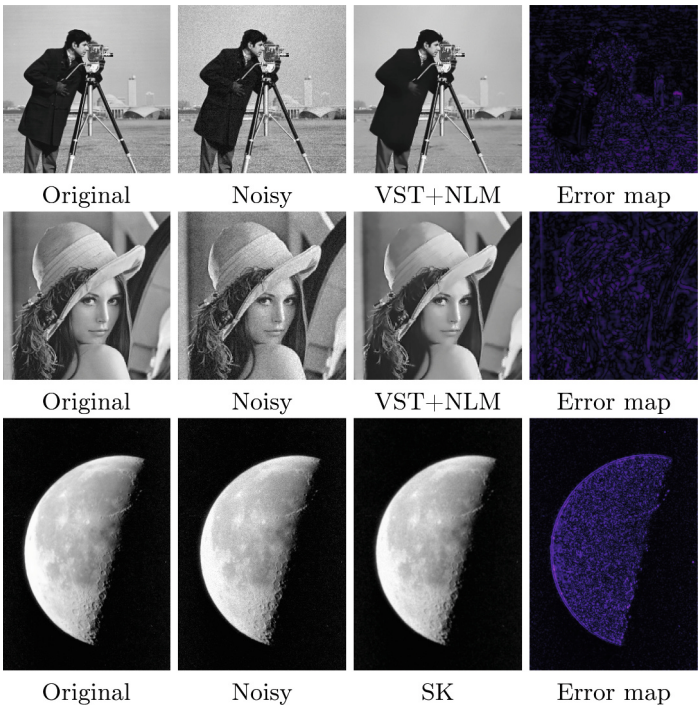

Fig. 6. On the left the reference images, in the center the image with Poisson noise and the best filtered images, on the right the ꟻLIP error map obtained.

As regards Speckle noise, Table 4 shows a more uniform distribution of best results across the competing methods. The BM3D filter achieves the best SSIM and RMSE values on the Autumn image, while the Frost filter ranks first on several other images in terms of SSIM, RMSE, and FSIM. Nevertheless, the NN and SK operators remain consistently close to the top performers, frequently appearing as the second-best method and never falling far behind the leader on any image or metric. This confirms their overall good applicability even in the presence of multiplicative noise. The error maps of the best filtering results are presented in Fig. 7.

Table 4. Results obtained filtering images corrupted by Speckle noise. Each row group corresponds to a reference image; the columns report the quality indices obtained comparing the reference image with each filtered version.

		BM3D	Lee	Frost	Log-Wiener	NN	SK
Autumn	↑ **SSIM**	0.8433	0.6196	0.6975	0.6698	0.6938	0.6883
	↓ **RMSE**	0.0408	0.0655	0.0555	0.0548	0.0525	0.0535
	↑ **FSIM**	0.9152	0.7663	0.8129	0.8156	0.8231	0.8226
	↓ **HLIP**	0.1034	0.1332	0.1231	0.1284	0.1197	0.1194
Cameraman	↑ **SSIM**	0.6535	0.6415	0.7008	0.6889	0.6391	0.6361
	↓ **RMSE**	0.0470	0.0687	0.0563	0.0503	0.0595	0.0613
	↑ **FSIM**	0.8743	0.7689	0.8253	0.8370	0.8031	0.7980
	↓ **HLIP**	0.0854	0.1219	0.1137	0.1085	0.1206	0.1258
Lena	↑ **SSIM**	0.7692	0.7196	0.7765	0.7425	0.7522	0.7430
	↓ **RMSE**	0.0426	0.0555	0.0484	0.0475	0.0494	0.0497
	↑ **FSIM**	0.9043	0.8431	0.8779	0.8752	0.8718	0.8699
	↓ **HLIP**	0.0862	0.1127	0.1043	0.1043	0.1079	0.1074
Moon	↑ **SSIM**	0.8642	0.8648	0.8881	0.7670	0.8755	0.8811
	↓ **RMSE**	0.0281	0.0277	0.0247	0.0468	0.0304	0.0264
	↑ **FSIM**	0.9045	0.8918	0.9118	0.8297	0.8865	0.9000
	↓ **HLIP**	0.0460	0.0525	0.0492	0.0525	0.0570	0.0523
Onion	↑ **SSIM**	0.7491	0.8145	0.8396	0.7761	0.8175	0.7992
	↓ **RMSE**	0.0369	0.0358	0.0323	0.0389	0.0404	0.0422
	↑ **FSIM**	0.8899	0.8807	0.8988	0.8853	0.8733	0.8786
	↓ **HLIP**	0.0871	0.0920	0.0888	0.0923	0.1068	0.1043

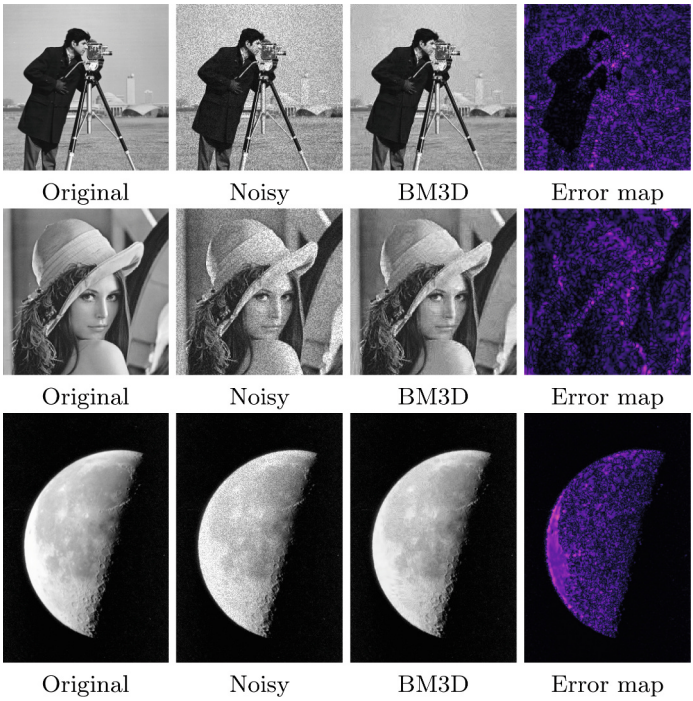

Fig. 7. On the left the reference images, in the center the image with Speckle noise and the best filtered images, on the right the ꟻLIP error map obtained.

Overall, the reconstructions obtained using NN and SK operators proved to be highly competitive across all three noise types considered. They achieved the best results in the Gaussian noise scenario, remained strong second-best alternatives in the Poisson case—where VST+NLM held the edge—and demonstrated solid performance under Speckle noise, where classical filters such as Frost showed a slight advantage. Even in these latter scenarios, the performance gap between operator-based methods and classical filters remains minimal, thus confirming the overall versatility and robustness of the proposed approximation-theoretic framework. These findings suggest that NN and SK operators represent promising alternatives to traditional denoising techniques, offering a more general and flexible approach that is not limited to a specific noise model. Future work may explore their application to other imaging tasks and their integration with hybrid filtering strategies.

Acknowledgments. The authors have been supported within the project "Mathematical Methods and Models for Biomedical Applications" financied by National Recovery and Resilence Plan PNRR-III-C9-2022-I8.

Disclosure of Interests. The authors have no competing interests to declare that are relevant to the content of this article.

References

1. Acu, A.M., Ilina, M., Sofonea, F., Travaglini, A., Vinti, G.: A comparison between neural network and sampling Kantorovich operators in terms of image denoising. In: Gervasi, O., et al. (eds.) ICCSA 2025. LNCS, vol. 15892, pp. 379–399. Springer, Cham (2026). https://doi.org/10.1007/978-3-031-97638-4_24
2. Andersson, P., Nilsson, J., Akenine-Möller, T., Oskarsson, M., Åström, K., Fairchild, M.D.: FLIP: a difference evaluator for alternating images. Proc. ACM Comput. Graph. Interact. Tech. **3**(2), 1–23 (2020)
3. Anscombe, F.J.: The transformation of Poisson, binomial and negative-binomial data. Biometrika **35**(3/4), 246–254 (1948)
4. Bardaro, C., Butzer, P.L., Stens, R.L., Vinti, G.: Kantorovich-type generalized sampling series in the setting of orlicz spaces. Sampl. Theory Signal Image Process. **6**(1), 29–52 (2007)
5. Brunet, D., Vrscay, E.R., Wang, Z.: On the mathematical properties of the structural similarity index. IEEE Trans. Image Process. **21**(4), 1488–1499 (2011)
6. Buades, A., Coll, B., Morel, J.M.: A non-local algorithm for image denoising. In: Proceedings of the IEEE Computer Social Conference on Computing Vision Pattern Recognition (CVPR), vol. 2, pp. 60–65 (2005)
7. Cao, F., Chen, Z.: The approximation operators with sigmoidal functions. Comput. Math. Appl. **58**(4), 758–765 (2009)
8. Cao, F., Chen, Z.: The construction and approximation of a class of neural networks operators with ramp functions. J. Comput. Anal. Appl. **14**(1), 101–112 (2012)
9. Cardaliaguet, P., Euvrard, G.: Approximation of a function and its derivative with a neural network. Neural Netw. **5**(2), 207–220 (1992)
10. Cheang, G.: Approximation with neural networks activated by ramp Sigmoids. J. Approx. Theory **162**, 1450–1465 (2010)
11. Cluni, F., Gusella, V., Vinti, G.: Masonry elastic characteristics assessment by thermographic images. Meccanica **54**(9), 1339–1349 (2019). https://doi.org/10.1007/s11012-019-00982-9
12. Corso, R., Vinti, G.: Mean sampling Kantorovich operators: approximation results and applications. Rev. Real Acad. Cienc. Exactas Fis. Nat. Ser. A-Mat. **120**, 36 (2026). https://doi.org/10.1007/s13398-026-01829-1
13. Costarelli, D., Vinti, G.: Approximation by multivariate generalized sampling kantorovich operators in the setting of orlicz spaces. Boll. Unione Mat. Ital. (9) **IV**, 14–20 (2011)
14. Costarelli, D., Vinti, G.: Convergence for a family of neural network operators in Orlicz spaces. Math. Nachr. **290**(2–3), 226–235 (2017)
15. Cybenko, G.: Approximation by superpositions of a sigmoidal function. Math. Control Sig. Syst. **2**, 303–314 (1989)
16. Dabov, K., Foi, A., Katkovnik, V., Egiazarian, K.: Image Denoising by Sparse 3-D Transform-Domain Collaborative Filtering. IEEE Trans. Image Process. **16**(8) (2007)
17. Frost, V.S., et al.: A model for radar images and its application to adaptive digital filtering of multiplicative noise. IEEE Trans. Pattern Anal. Mach. Intell. **4**(2), 157–166 (1982)
18. Gonzales, R.C., Woods, R.E.: Digital Image Processing. Addison Wesley (1992)
19. Jaybhay, J., Shastri, R.: A study of Speckle Noise reduction filters. Signal Image Process.: Int. J. (SIPIJ) **6**(3) (2015)

20. Kyurkchiev, N., Markov, S.: Sigmoid functions: some approximation and modelling aspects, some moduli in programming environment mathematica. LAP Lambert Acad. Publ. **4**, 34 (2015)
21. Lee, J.S.: Digital image enhancement and noise filtering by use of local statistics. IEEE Trans. Pattern Anal. Mach. Intell. **2**(2), 165–168 (1980)
22. Longaroni, M., Rinelli, L., Travaglini, A., Vinti, G.: Mathematical models and algorithms for processing retinal OCTA images. In: Gervasi, O., et al. (eds.) ICCSA 2025. LNCS, vol. 15892, pp. 358–378. Springer, Cham (2026). https://doi.org/10.1007/978-3-031-97638-4_23
23. Mäkinen, Y., Azzari, L., Foi, A.: Collaborative filtering of correlated noise: exact transform-domain variance for improved shrinkage and patch matching. IEEE Trans. Image Process. **29** (2020)
24. Makitalo, M., Foi, A.: Optimal inversion of the generalized Anscombe transformation for Poisson-Gaussian noise. IEEE Trans. Image Process. **22**(1), 91–103 (2013)
25. Rinelli, L., Travaglini, A., Vescera, N., Vinti, G.: Sampling type operators versus AI in medical image processing. Discrete Contin. Dyn. Syst. Ser. S (2025). https://doi.org/10.3934/dcdss.2025147
26. Tomasi, C., Manduchi, R.: Bilateral filtering for gray and color images. In: Proceedings of the 6th International Conference on Computer Vision, pp. 839–846 (1998)
27. Travaglini, A., Vinti, G.: A mathematical model for the analysis of eye fundus images in healthy and diabetic patients. In: Gervasi, O., et al. (eds.) ICCSA 2023. LNCS, vol. 14108, pp. 558–576. Springer, Cham (2023). https://doi.org/10.1007/978-3-031-37117-2_38
28. Travaglini, A., Vinti, G., Scalera, G.B., Scialpi, M.: A large scale analysis for testing a mathematical model for the study of vascular pathologies. Mathematics **11**(8), 1–19 (2023)
29. Wang, Z., Bovik, A.C., Sheikh, H.R., Simoncelli, E.P.: Image quality assessment: from error visibility to structural similarity. IEEE Trans. Image Process. **13**(4), 600–612 (2004)
30. Wiener, N.: Extrapolation, Interpolation, and Smoothing of Stationary Time Series: With Engineering Applications. Wiley (1949)
31. Zaabouli, Z., Afraites, L., Laghrib, A., Hadri, A.: Gaussian and Poisson noise identification using non-convex optimization with L^2-norm power constraints. ESAIM Math. Model. Numer. Anal. **59**(3), 1705–1727 (2025). https://doi.org/10.1051/m2an/2025043
32. Zhang, L., Zhang, L., Mou, X., Zhang, D.: FSIM: a feature similarity index for image quality assessment. IEEE Trans. Image Process. **20**(8) (2011)